Parametric Study on Slosh-Induced Impact Pressures: Experiment vs. Numerical Computation

Young-Bum Lee[(1)], Younghwan Kim[(2)], Yong-Soo Kim[(1)], Young-Sup Shin[(3)]

[(1)] Ship and Ocean Research & Development Institute, Daewoo Shipbuilding & Marine Engineering Co., Koje, Korea

[(2)] Department of Ocean Engineering, MIT, Cambridge, MA, USA

[(3)] Research Department, American Bureau of Shipping, Houston, TX, USA

Introduction

There is presently an increasing need for accurate sloshing analysis due to the designs of new LNG carriers and floating production-storage-offloading platforms (FPSOs). The LNG carriers currently under construction and planning are significantly larger than those built in the 1970s and 1980s, and about 70% of current designs adopt the membrane-type LNG cargo tanks which have a greater potential for severe sloshing impact occurrence. The sloshing problem is also critical for FPSOs. Since there is no restriction on the filling ratio for FPSO cargo tanks, the probability of resonance between sloshing and wave excitation is very high. In such cases, the accurate prediction of slosh-induced pressures is essential for the design of safe internal structures.

Despite the many reports on sloshing experiments, systematic experimental data available in the public domain are very limited. In particular, this is the case for slosh-induced impact pressures on the tank ceilings and/or walls, which are of great practical interest. In the present study, we introduce a set of experimental data for rectangular tanks, especially measured impact pressure on the tank ceiling.

The sloshing problem is a well-defined problem with a finite domain. However, practical interest focuses generally on cases of violent flows, when the safety of ship structure is concerned. Because of the strong nonlinearity of free surface and frequent contact with the tank boundary, a numerical simulation of violent sloshing flow is a challenging task. One of difficulties of applying numerical methods is the strong sensitivity of computational parameters, *e.g.* time segment and mesh size. This sensitivity is critical to an accurate prediction of slosh-induced impact pressure. In the present study, we have carried out a parametric study to observe the sensitivity in the application of a finite difference method.

Experimental Data for Rectangular Tanks

For the parametric study, we consider a set of unpublished experimental data for two rectangular tanks shown in Fig.1. The model tests were carried out at the Research Center of Hitachi Zosen in 1991 under the support of, and as in collaboration with Daewoo. A series of tests were conducted for forced harmonic surge excitations with different motion amplitudes and frequencies at several filling conditions. Strain-gage sensors with the measuring ranges of 0.2 kgf/cm^2 and 0.5 kgf/ cm^2 were installed at nine locations on the tank ceiling, side wall, and internal members to measure the time-signals of hydrodynamic pressures, and a displacement sensor and an accelerometer were also used to check the accuracy of the excitation.

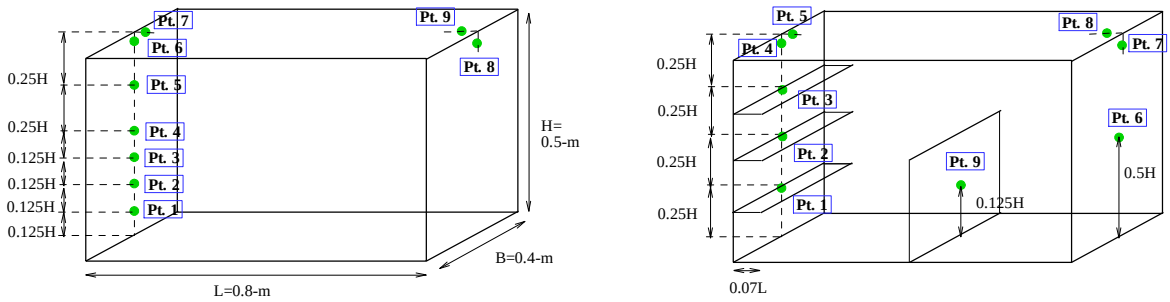

Figure 1. Two test models and the location of sensors: left; Tank A, right; Tank B

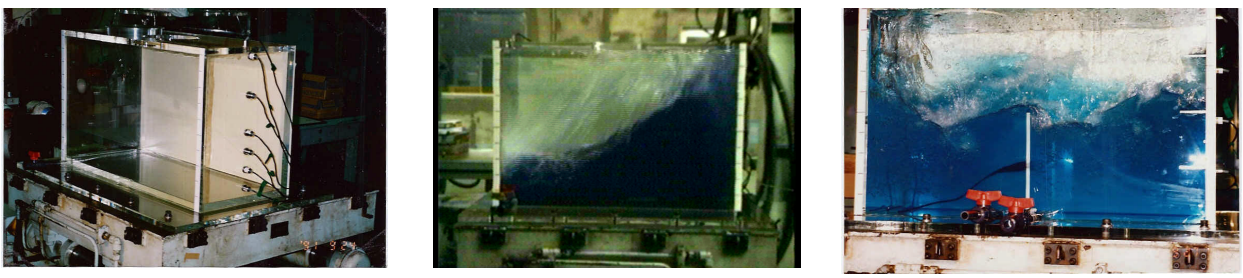

Figure 2. Tank-A with pressures Sensors and snapshots of sloshing flows under excitation

Fig.2 shows snapshots of sloshing flows in the two tanks. The peak pressures were obtained from the measured pressure histories digitized for approximately 10 seconds with 4-msec interval. The measured peak pressures on the tank ceiling are summarized in Table 1.

Filling Ratio	Excitation Freq. / Natural Freq.	Peak Pressure (kN/m^2)			
		Motion Displacement: 2-cm		Motion Displacement: 4-cm	
		Tank A (Pt.7/9)	Tank B (Pt.8)	Tank A (Pt.7/9)	Tank B (Pt.8)
30%	0.8	0.08 / 0.71	0.07	0.08 / 0.75	1.53
	0.9	0.08 / 0.08	0.34	4.06 / 1.73	0.36
	1.0	0.18 / 0.30	1.12	1.57 / 2.43	0.18
	1.1	9.97 / 7.17	0.18	2.35 / 3.31	0.22
	1.2	0.00 / 0.18	0.84	4.25 / 6.94	0.38
50%	0.8	0.08 / 0.32	0.74	0.12 / 0.30	0.73
	0.9	0.08 / 0.32	0.13	16.25 / 3.21	-
	1.0	9.87 / 14.64	1.12	40.08 / 16.66 (*)	0.77
	1.1	0.29 / 0.09	0.75	1.27 / 6.10	0.79
	1.2	0.10 / 0.39	0.18	0.10 / 0.54	1.29
70%	0.8	0.35 / 0.30	0.06	0.35 / 0.30	0.07
	0.9	0.08 / 0.32	0.06	9.97 / 11.10	0.28
	1.0	5.64 / 9.43	0.07	16.44 / 11.27	0.71
	1.1	1.76 / 3.93	0.07	7.85 / 7.79 (*)	0.11
	1.2	0.00 / 0.25	0.07	24.67 / 1.52 (*)	0.20
80%	0.8	0.03 / 0.22	0.13	2.86 / 27.41 (*)	2.20
	0.9	6.55 / 8.14	0.04	5.14 / 6.82	1.82
	1.0	3.82 / 3.94	0.07	7.38 / 9.07	1.91
	1.1	5.51 / 0.76	0.13	11.46 / 9.92	1.29
	1.2	0.03 / 0.26	0.11	22.41 / 24.52	1.96

Table 1. Summary of peak pressures on the tank ceiling of DAEWOO Model (*; need more careful observation)

Numerical Computation: a Sensitivity Study

The finite difference method applied by Kim (2001, 2002) is employed in the present parametric study. This method is based on the SOLA-SURF method which assumes the single-valued free surface profiles. In particular, for the prediction of impact pressure on the tank ceiling, some representative schemes have been applied - *e.g.* buffer zone, time-averaging, and proper detachment of the fluid from the tank ceiling. In this study, focusing on the Euler equation, the sensitivities of the computed impact pressure to the computational parameters, such as time segment, mesh size, size of buffer zone, and time-averaging interval, are observed.

Within the buffer zone below the tank ceiling, the boundary condition on the free surface takes the following form:

$$F = k\frac{p - p_{atm}}{r} + (1-k)\frac{H_B}{\Delta t}V_N = 0 \tag{1}$$

where κ is the weight of the free surface boundary condition and H_B is the size of the buffer zone. In addition, p, p_{atm}, r, V_N are pressure, gas pressure above the free surface, the fluid density, and the normal velocity on the wall, respectively. Kim (2001) set κ as $(\eta_{\max} - \eta)/H_B$ where η is free-surface elevation and $\eta_{\max}$ is the maximum possible elevation, i.e. height of the tank ceiling. We apply the same weight of the free surface boundary condition, then H_B becomes a critical parameter.

Due to the discretization of computational domain in the finite difference method, a computed pressure signal can have a series of spikes. To render it more smooth/continuous (for application to structural analysis or comparison with a measured signal), a time-averging scheme is applied. The averaged pressure can be written as

$$P_{avg}\left(t_{avg}\right) = \frac{1}{\Delta T}\sum_{n=1}^{N} P(t^{(n)})\Delta t^{(n)} \qquad \text{where} \quad t_{avg} = t^{(n)} + \frac{\Delta T}{N} \quad \text{and} \quad \Delta T = \sum_{n=1}^{N}\Delta t^{(n)} \ . \tag{2}$$

Then, the magnitude of peak pressure may be sensitive to the number of averaging data point, *N*.

Fig.3 shows three snapshots of sloshing flow at an 80% filling condition, comparing the computational results with the actual free-surface profiles. With the exception of some water splash and jets, a fair agreement is shown. The dependency of peak pressure on mesh size is shown in Fig.4. In this present case, all computational parameters except for the number of solution meshes are fixed, and the vertical mesh sizes are adjusted proportionally to the horizontal

mesh sizes. In this case, the time segment has been chosen enough small to provide convergent solutions. A strong sensitivity to mesh size is not shown in this figurg, and it is probably owing to the application of buffer zone. Fig.5 shows the computed peak pressures with and without time-avergaing for different time segments. In this specific case, a smaller pressure is obtained generally for a larger time segment. Furthermore, when time segment is large, the magnitude of peak pressure is stongly dependent on the interval of time-averaging. However, when the time segment is smalle, a certain convergence can be observed, especially when the time-averging scheme is applied.

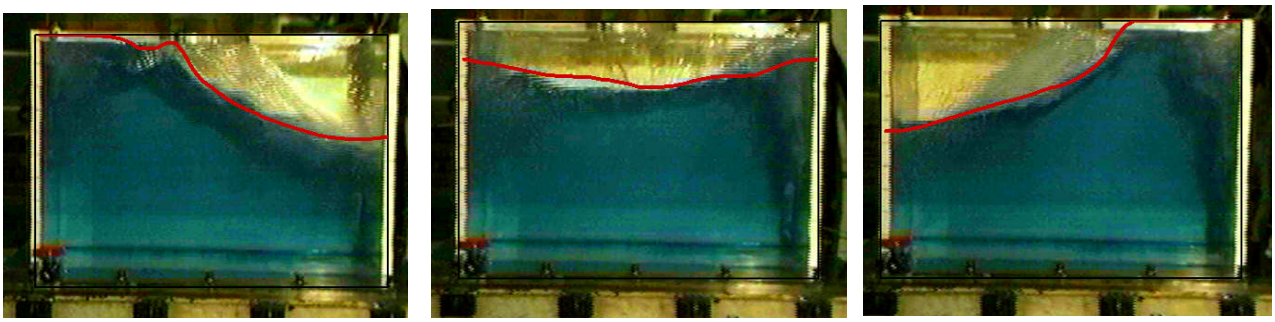

Figure 3. Comparisons of free-surface profiles between expriment and computation (thick line);Tank-A, 80% filling, 4-cm amp., 0.955-Hz

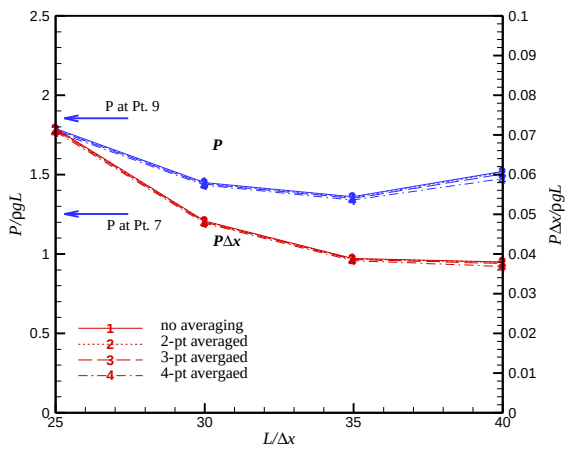

Figure 4. Peak pressures for different meshes: Tank A, 50% filling, 2-cm amp., 0.858-Hz, observed time window; $60 \le t\sqrt{g/L} \le 120$, $\Delta t\sqrt{g/L} = 1\times10^{-3}$

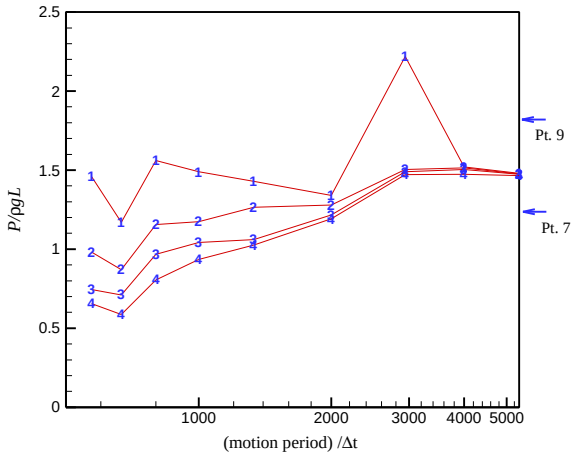

Figure 5. Peak pressures for different time segment: same condition with Fig.4, 40x25 meshes.

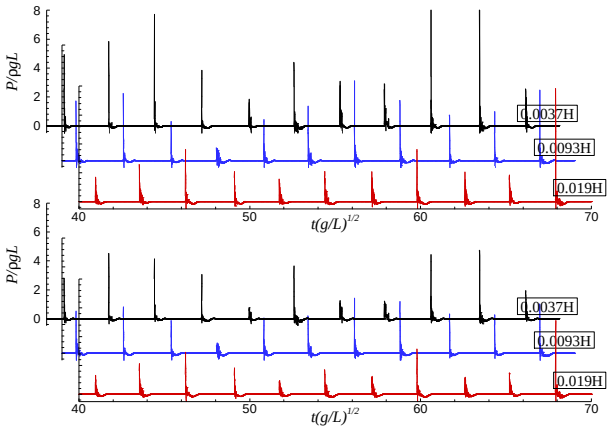

Figure 6. Time-histories of pressure on the tank ceiling for different sizes of buffer zone: Tank A, 80% filling, 4-cm amp., 1.23-Hz, 40x25 meshes, top; no averaging, bottom; 3-pt. averaged, experiment; 2.85(Pt.7), 3.12(Pt.9)

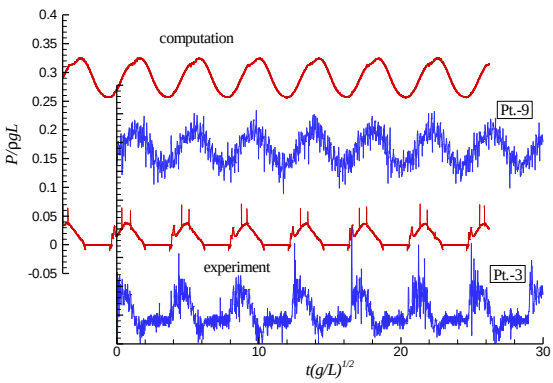

Figure 7. Comparison of time-histories of pressure: Tank B, 70% filling, 2-cm amp., 0.835-Hz, 40x28 meshes

Fig.6 shows the pressure histories for different height of buffer zone. As expected, larger impact pressures are observed for smaller height. Although it is found that the time-averaging scheme mitigates the sensitivity to buffer-zone

height, it seems that a short heights results in significant over-prediction of impact pressures. Fig.7 compares the measured and computed pressure signals for Tank B. Overall trend trends are similar, but some discrepancy is found in corner area under horizontal internal members.

Extension of Buffer Zone to Chamfers

The concept of buffer zone can be extended to sloping boundaries, especially for the upper chamfer. For the sloping boundary as Fig.8, we can substitute

$$p - p_{atm} = p_{ijk}\left(\frac{\eta_{ij} - z_{k-1}}{\Delta z} + \frac{1}{2}\right) - p_{ijk-1}\left(\frac{\eta_{ij} - z_{k-1}}{\Delta z} - \frac{1}{2}\right) \quad (3)$$

$$V_N \approx \frac{1}{2}(u_{ijk} + u_{i-1jk})\sin\theta - \left\{w_{ijk-1} - \frac{\Delta z}{\Delta x}\left(u_{ijk} - u_{i-1jk}\right)\right\}\cos\theta \quad (4)$$

into equation (1). Furthermore, equation (1) can be solved using Newton-Rapson method, i.e.

$$\Delta p = -F/(dF/dp) \quad (5)$$

where

$$\frac{dF}{dp} = \frac{z_k - \eta_{ij}}{H_B}\left(\frac{\eta_{ij} - z_{k-1}}{\Delta z} + \frac{1}{2}\right) + \left(1 - \frac{z_k - \eta_{ij}}{H_B}\right)\frac{H_B}{\Delta t}\left(\frac{1}{\Delta z} + \frac{2\Delta z}{\Delta x^2}\right)\cos\theta \cdot \quad (6)$$

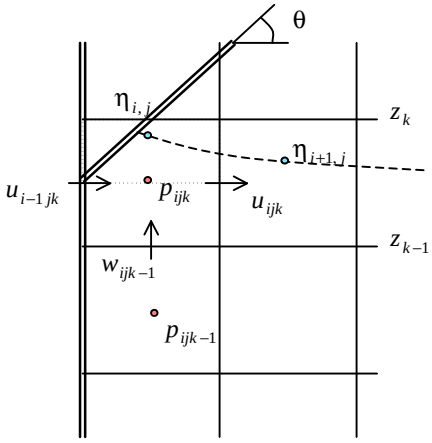

Figure 8. Buffer zone near chamfer

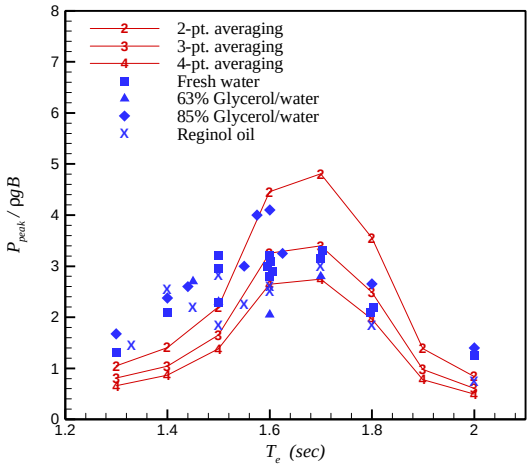

Figure 9. Impact pressures at the upper knuckle point: tank model; Abramson *et al.* (1974), *h/B*=0.40, sway amplitude=B/10

Fig.9 compares the computed peak pressures with experimental data for the tank shape introduced by Abramson *et al.* (1974). In this case, the quantities are 1/10 exceedance values and water has been assumed in numerical computation. The computational results show some dependency on the time-averaging interval, but overall agreement with experimental data is fair. Fig.10 shows the computed pressure time-histories at the center of a three-dimensional prismatic tank with ength-beam ratio of 1.5 and depth-beam ratio of 1.0. The sloshing flows in three-dimensional prismatic tanks are much more complicated than those in two-dimensional tanks. Fig.10 compares the computed pressure signals at the corners of the tank ceiling with two-dimensional rectangular case. Due to sloping boundary, three-dimensional flows cause significantly higher impact pressures.

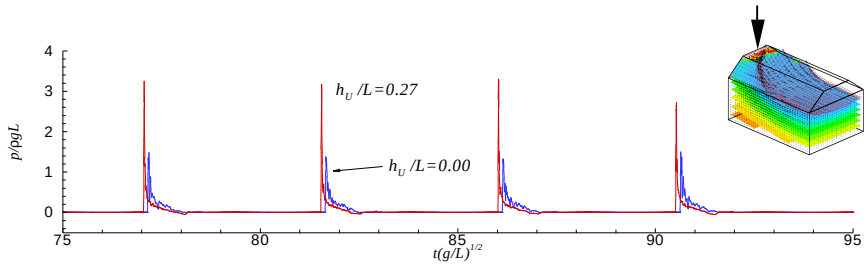

Figure 10. Time-histories of hydrodynamic pressure at an edge of tank top: *(x,y,z)=(-L/2,0,H)*, 3-point averaging, *L/B*=1.5, *H/B*=1.0, *h/H*=0.7, height of upper chamfer=0.27*H*, 10-deg pitch, excitation period= $4.49\sqrt{L/g}$.

References

Kim, Y., Numerical simulation of sloshing flows with impact load. Applied Ocean Research, Vol.23, 2001.

Kim, Y., A Numerical Study on Sloshing Flows Coupled with the Ship Motion; Anti-Rolling Tank Problem. Jour Ship Research, Vol. 46, 2002.

Kim, Y, Shin, Y., Lee, K., Numerical study on slosh-induced impact pressures on three-dimensional prismatic tanks (submitted for publication)

Abramson, R.L, Bass, R.L., Faltinsen, O.M., Olsen, H.A., Liquid sloshing in LNG carriers, 10th ONR Symposium, 1974.

Development of systematic sloshing-analysis program II, Research Report SH-9121, DAEWOO, 1993.